RESEARCH PAPER

PCCP
www.rsc.org/pccp

Density functional theory study of the oxidation of CO by OH on Au(110) and Pt(111) surfaces

Tatyana E. Shubina,* Christoph Hartnig† and Marc T. M. Koper*

Schuit Institute of Catalysis, Laboratory of Inorganic Chemistry and Catalysis, Eindhoven University of Technology, 5600 MB, Eindhoven, The Netherlands. E-mail: T.E.Shubina@tue.nl, M.T.M.Koper@tue.nl

Received 21st May 2004, Accepted 9th June 2004
First published as an Advance Article on the web 24th June 2004

Results of a periodic density-functional theory study of the adsorption of carbon monoxide (CO), hydroxyl (OH), and carboxyhydroxyl (COOH) on Au(110) and Pt(111) surfaces are presented, including their binding energetics, binding geometry, and vibrational characteristics. The reaction pathway and activation barrier for COOH formation from CO and OH on both surfaces are also computed and compared. The relationship between our findings and previous experimental and theoretical results are discussed, particularly in connection with the striking CO electro-oxidation capability of (single-crystal) gold electrodes.

Introduction

The catalytic oxidation of carbon monoxide is one of the most important catalytic reactions in both heterogeneous and homogeneous media. In heterogeneous gas-phase catalysis, CO oxidation plays an essential role in the "water–gas shift" reaction,[1,2] whereby CO reacts with water with formation of carbon dioxide and hydrogen, and in the removal of CO by oxidation with dioxygen in catalytic car exhaust converters.[3,4]

Electrooxidation of CO is a process analogous to the water–gas shift reaction in which CO_2 and hydronium ions form by oxidation with water at the metal–water interface. Adsorbed CO is also a common reaction intermediate in the electrooxidation of methanol and other organic feedstocks, which are used in fuel-cell technology. There have also been numerous studies of the water–gas shift reaction carried out homogeneously by transition-metal complexes in aqueous media.[5]

It has been known for a long time that the oxidation of CO could be effectively catalyzed by certain transition metals.[6] There are many experimental and theoretical studies on the catalytic oxidation of CO over platinum group metals (for a recent review, see *e.g.* ref. 7). It was long believed that gold failed as a catalyst. However, the oxidation of hydrogen on a gold gauze was observed as early as 1906.[8] The earliest reference to gold as a catalyst for carbon monoxide oxidation dates from 1925.[9] Recent studies showed that Au, deposited as small particles on reducible and non-reducible metal oxides, is an excellent catalyst for CO oxidation at low temperatures.[7,10] There is no consensus yet as to the exact physical origin of the catalytic activity of these supported gold particles: though some authors relate it to the special activity of the contact interface between the gold particles and the oxide support,[10] others adhere to the special activity of the "quantum-sized" gold particles as stabilized by their interaction with the oxide.[7] Recent density functional theory (DFT) studies seem to provide support in favour of both interpretations.[11]

The electrochemical oxidation of CO is mainly of interest in fuel cell technology. An important issue in contemporary fuel cell electrocatalysis is to develop new materials that can oxidize CO at low overpotentials, or adsorb only a small amount of CO while still capable of oxidizing hydrogen. The current state-of-the-art CO tolerant catalyst consists of platinum modified by second or third metal, such as ruthenium.[12,13] In relation to fuel cell catalysis, the electrochemical oxidation of carbon monoxide on (modified) platinum has been extensively studied over the past decades. The generally accepted "reactant-pair" mechanism proposed by Gilman[14] assumes a Langmuir–Hinshelwood (LH) type reaction between adsorbed carbon monoxide and an oxygen-containing surface species. Despite the fact that the exact nature of the oxygen-containing species is still unknown most of the authors write it as surface-bonded OH. In reaction equations, this mechanism reads as:

$$H_2O + * \rightleftharpoons OH_{ads} + H^+ + e^- \quad (1)$$

$$OH_{ads} + CO_{ads} \rightarrow 2* + CO_2 + H^+ + e^- \quad (2)$$

Many previous publications[15–18] as well as recent experimental work[19] from our group have demonstrated the validity of the LH mechanism for both the CO adlayer oxidation on stepped Pt[n(111) × (111)] electrodes and for the continuous CO oxidation on rotating platinum electrodes,[20] with a competitive adsorption of the two reactants, CO and OH. The LH mechanism has also been invoked to explain the CO oxidation kinetics on other transition-metal electrodes such as Ru,[21,22] Rh[23] and Pd.[24] For the CO adlayer oxidation on platinum, a Tafel slope of 75 ± 3 mV dec^{-1} has been reported, irrespective of the platinum surface structure.[25] As suggested by Santos *et al.*[26] and Herrero *et al.*,[27] such a value of the Tafel slope could be interpreted in terms of the following, more detailed mechanism:

$$H_2O + * \rightleftharpoons OH_{ads} + H^+ + e^- \quad (1)$$

$$OH_{ads} + CO_{ads} \rightarrow COOH_{ads} \quad (3)$$

$$COOH_{ads} \rightarrow 2* + CO_2 + H^+ + e^- \quad (4)$$

In fact, the involvement of a hydroxylcarbonyl radical intermediate was postulated in Gilman's original paper.[14] Spectroscopic evidence for the formation of surface-bonded COOH species in the electrochemical oxidation of a CO adlayer on Pt was reported by Watanabe *et al.* using infrared spectroscopy in the attenuated total reflection mode,[28,29] from the observation of a weak band between 1300–1500 cm^{-1}. On the basis of infrared spectra of stable transition-metal hydroxycarbonyl

† Present address: Research Center "Juelich", Institute for Materials and Processes in energy systems (IWV-3), D-52425 Juelich, Germany.

DOI: 10.1039/b407669a

complexes, a band is expected near 1600 cm^{-1}. However, considering that this is the spectral region of the water bending vibrations, the unequivocal identification of this band requires experiments in deuterated water.

As in the gas-phase, gold is also known to be an excellent catalyst for CO oxidation under electrochemical conditions, both in acidic and alkaline solutions. Interestingly, the electrochemical CO oxidation may take place at single-crystal gold without the need for an oxidic support, suggesting fundamentally different properties of gold under electrochemical conditions compared to the gas-phase. Detailed investigations of the electrochemical CO oxidation on gold were published by Weaver *et al.*[30] In acidic solution, they suggested the following mechanism:

$$CO_{ads} + H_2O \rightleftharpoons COOH_{ads} + H^+ + e^- \quad (5)$$

$$COOH_{ads} \rightarrow CO_2 + H^+ + e^- \quad (4)$$

This mechanism was suggested on the basis of the observed pH dependence in acidic and alkaline solution and the near unity reaction order in CO solution concentration. In contrast to CO oxidation on Pt, there is no competitive adsorption between reactants, which is related to the low adsorption energy of CO on Au. However, as noted by Weaver *et al.*, the observed Tafel slope of *ca.* 120 mV dec^{-1} is difficult to interpret in terms of the above mechanism, as it suggests a rate-determining first electron transfer step. Another important difference between CO oxidation on Au and Pt, as noted by Weaver *et al.*, is the observation that on Au CO oxidation is catalyzed at potentials markedly below those corresponding to the initial formation of adsorbed hydroxyl, whereas on Pt the onset of CO oxidation essentially coincides with the initial formation of adsorbed hydroxyl. This suggests a stabilization of surface-bonded OH by adsorbed CO, or the direct formation of a COOH species without the need of forming the surface-bonded hydroxyl. Such stabilization was in fact suggested by the SERS experiments of the Weaver group, which indicated the formation of a surface-bonded oxygen species on gold in the presence of CO, which was not observed in the absence of CO. However, Blizanac *et al.* have recently suggested that the real onset potential for OH adsorption is *ca.* 0.3 V lower than the onset potential suggested by voltammetry or surface-enhanced Raman spectroscopy, explaining the unexpected reactivity for CO oxidation at these low potentials.[31]

Given the apparent importance of the surface-bonded COOH species in the mechanism of electrochemical CO oxidation, we have undertaken detailed density-functional theory (DFT) calculations of CO, OH, and COOH adsorption and formation on gold and platinum surfaces. We have chosen the Au(110) and Pt(111) surfaces as the two low-index planes most typically studied for CO oxidation. Our purpose is to provide mechanistic insight into the CO oxidation reaction on gold and platinum electrodes by providing the relevant energetics of COOH formation and adsorption. In particular, we want to address the questions of why gold is such a good CO electrooxidation catalyst (even in acidic solution), without the need for nano-sized particles or support interactions, and what could be the possible differences in reaction mechanism on Pt and Au suggested by these calculations. We note that similar DFT-based calculations have been published recently by Anderson and Neshev[32] and by Saravanan *et al.*[33] for COOH formation on small Pt clusters, as well as by Ishikawa *et al.* using a combination of DFT cluster calculations and bond-order conservation arguments.[34,35] Our DFT calculations are based on the slab geometry, which should give more reliable energetics, and specifically aim at comparing Pt and Au in order to resolve the seemingly disparate CO oxidation kinetics observed on these two electrode surfaces.

The paper is organized as follows. In the next section, the computational details are outlined. In the following sections, the adsorption energetics of CO, OH, COOH, and the energetics of formation of COOH from surface-bonded CO and OH are discussed separately for the Au(110) and Pt(111) surface. The results will be compared in a final section and discussed in terms of the above-mentioned mechanisms.

Computational methods

1. Slab approach

Periodic slab calculations were performed using the Vienna *ab initio* simulation package (VASP),[36–38] as described in ref. 39. Briefly, the surfaces were modeled as four-layer slabs, with the atomic distances fixed to the calculated bulk lattice distance, and a vacuum, corresponding to six (for (Au110)) and five (for Pt(111)) equivalent layers. The top metal layer was relaxed in all calculations. The (2 × 2) unit cell was used to model both Au(110) and Pt(111) surfaces. The computed CO, OH and COOH coverages were therefore 0.25 ML.

The adsorption of CO was always restricted to a perpendicular orientation, with the oxygen pointing away from the surface. The adsorption of OH was performed by allowing for a tilting of the O–H molecular axis, with the oxygen fixed to one of the high-symmetry sites and the hydrogen pointing away from the surface. M–C, C–O, M–O and O–H bond distances as well as OH tilting angles with the surface (α) were fully optimized.

The ground-state electronic energy was calculated using the density functional theory (DFT) formalism. The Kohn–Sham equations were solved in the so-called DFT-generalised gradient approximation (GGA). The Vosko–Wilk–Nusair[40] form of the local density approximation was used, in combination with the PW91 functional for the GGA.[41] The Kohn–Sham orbitals were expanded in a plane-wave[42] basis set and the interaction of the valence electrons with the ion cores was described by ultrasoft pseudopotentials.[43] The calculated lattice constants for bulk Au and Pt were found to be 4.18 and 3.96 Å, respectively, in reasonable agreement with the experimental values of 4.08 and 3.92 Å.[44] The plane-wave expansion was truncated at an energy cut-off of 350 eV and a grid of at least 7 × 5 × 1 for Au(110) and 7 × 7 × 1 for Pt(111) Monkhorst–Pack special *k*-points were used to perform the Brillouin-zone integrations. The binding energy was computed as the difference between the energy of the composite system and the sum of the energies of the clean surface and uncoordinated adsorbate. No spin polarisation effects were accounted for, except for the uncoordinated OH species, the energy of which was calculated in the spin-unrestricted mode.

To determine the reaction path and activation energy for the CO + OH reaction, a two-dimensional potential energy surface was computed by systematically changing the position of the OH within the unit cell, requiring that the CO remains at or near the atop adsorption site. All other remaining degrees of freedom were optimized at each energy calculation. From this two-dimensional potential energy surface, the reaction path was obtained, with the transition state (defining the activation energy) as the saddle point of the surface.

Vibrational frequencies were computed by two different methods. First, the ν_{M-CO} and ν_{CO} stretching frequencies were calculated from a potential energy surface (PES), consisting of 7–9 points, respectively, within a range of displacements of *ca.* ±0.20 Å using the AnharmND program.[45,46] A second approach to calculate the vibrational properties of the system is *via* the vibrational power spectrum, which can be obtained by Fourier transformation of the velocity autocorrelation function (vacf).[47] The latter can be obtained from *ab initio* molecular dynamics simulations, which were performed with the same program package VASP.

The *ab initio* molecular dynamics simulations were carried out using the same arrangement of atoms as described above;

however, in order to account for possible coupling effects and to reduce the statistical noise, the size of the unit cell was doubled in both directions of the surface plane. The starting geometry was taking from the static calculations with slightly elongated arrangements of the adsorbate. The Verlet integration scheme was used with a time step of 0.5 fs and no constraints to the molecular geometries of the adsorbate were applied. However, the substrate atoms were kept fixed. The temperature of the system was set to 300 K using the Nosé-thermostat in a microcanonical ensemble.

The functional setup was identical with the calculations described above, with the difference that only the Γ-point was used to perform the Brillouin zone integrations, which should be a reasonable simplification due to the larger size of the unit cell. The vacf was calculated following the standard scheme[47] with a correlation length $\tau = 1.5$ ps. The resulting correlation function was multiplied with a smoothing function $f(t)$ with $f(t) = \sqrt{(1-t)\tau}$ to achieve a properly vanishing correlation function. The Fourier transform of this vacf gives the vibrational power spectrum of the adsorbate layer.

2. Cluster approach

Density functional theory calculations for 9-atom (consisting of layers of 4, 1, and 4 atoms) Au and 10-atom (consisting of layers of 7 and −3 atoms) Pt clusters (see Fig. 1) were carried out with Gaussian98 program package.[48] Harmonic vibrational frequencies were computed with the BPW9141 functional. For C and O the 6-31G* basis set was employed, for H atom we used triple-zeta 6-311G** basis, for Au and Pt the LANL2DZ basis set with an effective core potential and double-zeta valence orbital. Different functionals (BLYP,[49,50] B3LYP[51]) and larger clusters were also used to validate the obtained vibrational frequencies. Frequency calculations were performed using optimized geometries from periodical DFT calculations. We should stress here that we used this approach in case of "complicated" molecules such as adsorbed COOH due to the time-consuming procedure of calculating the full multidimentional PES as input for the AnharmND program. Despite the fact that the optimized geometries that are minima in periodical calculations should not be the equilibrium geometries for the cluster calculations, comparison of the different results (see below) indicates that this approach still allows to obtain fairly accurate vibrational frequencies.

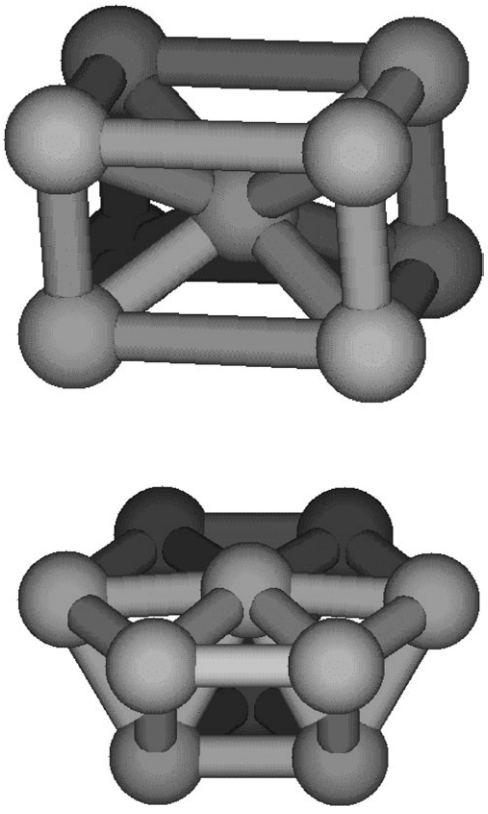

Fig. 1 The clusters used for Au(110) (top) and Pt(111) (below) surfaces.

Results and discussion

Au(110)

Adsorption of CO and OH on Au(110). The calculated binding energies, optimized bond distances and vibrational properties of adsorbed CO and OH on the various sites on the Au(110) surface are collected in Tables 1 and 2. Our calculations suggest that there are two preferred sites for CO adsorption on Au(110): the atop adsorption site and the short bridge site both with a binding energy of *ca.* 0.7 eV. The Au–C bond length for CO adsorbed atop is 1.98 Å, for bridged-bonded CO it is 1.48 Å. The C–O bond length in case of bridge-bonded CO is slightly elongated (1.167 Å) compared to the atop coordination (1.151 Å), in agreement with the lower C–O vibrational frequency observed in the short-bridge site.

The vibrational frequencies for atop- and bridge-bonded CO adsorbed computed using the slab and cluster approaches, as well as those obtained from the MD generated vibrational spectrum for atop adsorbed CO, are also compared in Table 1 (for uncoordinated CO, a stretching frequency of 2132 cm^{-1} was obtained with VASP[39]). The obtained frequencies generally agree quite well with experiment. For Au(110)/CO adsorbed atop a C–O stretching frequency of 2040–2100 cm^{-1} is found, whereas for bridge-bonded CO a vibrational frequency of *ca.* 1960 cm^{-1} is obtained. Literature values for the C–O stretching frequency, adsorbed at the top site on polycrystalline Au, fall within the range of 2000–2100 cm^{-1}. Beden *et al.*[52] reported in an IR study the presence of linearly bonded (close to 2120 cm^{-1}) and bridge-bonded (1930 cm^{-1}) CO at Au in 1 M $HClO_4$. Tadayyoni and Weaver[53] reported a value of 2080–2150 cm^{-1} for the C–O stretching frequency obtained by the SERS method. Later, Zhang and Weaver[54] reported a ν_{CO} of 2115 cm^{-1} obtained by the same method.

Table 2 gives the results obtained for OH adsorbed on the different sites of the Au(110) surface. It is found that OH preferentially adsorbs on the short bridge site with a tilting

Table 1 Binding properties of CO on Au(110)

				anh(VASP)		harm(G98)		MD
Adsorption site	Binding energy/eV	r(Au–C)/Å[a]	r(C–O)/Å	ν_{AuC}/cm^{-1}	ν_{CO}/cm^{-1}	ν_{AuC}/cm^{-1}	ν_{CO}/cm^{-1}	ν_{CO}/cm^{-1}
atop	−0.691	1.983	1.151	310	2042	338	2102	2070
bridge short	−0.673	1.478	1.167	248	1962	255	1959	—
bridge long	−0.070	1.737	1.153	—	—	—	—	—
hollow	0.067	1.817	1.149	—	—	—	—	—

[a] The M–C distance refers to the perpendicular distance from the first metal layer. The same holds for the Au–O, Au–C, Pt–C and Pt–O columns in Tables 2, 3, 5, 6 and 7.

Table 2 Binding properties of OH on Au(110)

Adsorption site	Binding energy/eV	r(Au-O)/Å	r(O-H)/Å	α
atop	−2.239	2.067	0.976	108.6
bridge short	−2.499	1.615	0.976	111.1
bridge long	−2.188	1.145	0.978	123.6
hollow	−1.780	1.122	0.981	166.0

Table 3 Binding properties of COOH on Au(110)

Adsorption site	Binding energy/eV	r(Au–C)/Å	r(C–O_1)/Å	r(C–O_2)/Å	r(O_2–H)/Å
$CO_1O_2H_{free}$	—	—	1.198	1.331	0.990
CO_1O_2H	−1.78	2.095	1.212	1.366	0.988

angle of *ca.* 111° to the surface. The other adsorption sites are considerably less favourable.

Adsorption of COOH on Au(110). The computed binding characteristics (VASP) and vibrational properties (VASP-MD, Gaussian 98) of adsorbed COOH on Au(110) are collected in Tables 3 and 4. The same table also gives the Gaussian 98 computed bond lengths. Fig. 2 shows the vibrational power spectrum of COOH as obtained from an *ab initio* molecular dynamics run with VASP. It is found that COOH prefers to adsorb on Au(110) with the carbon atom coordinated to a single Au surface atom with a binding energy of −1.78 eV relative to the uncoordinated COOH. Vibrational frequencies for the uncoordinated COOH are collected in Table 4. From the vibrational frequencies calculated for uncoordinated COOH and the typical spectral regions for monomeric carboxylic acid, the modes at 1000–1100, 1250–1300, 1700–1850, and 3500–3600 cm^{-1} may be identified as the C–OH stretching mode, the O–H bending mode, the C–O stretching mode, and the O–H stretching modes, respectively. For COOH adsorbed on Au(110) we also obtain a vibration mode at 249 cm^{-1} corresponding to the Au–C(OOH) stretching mode. In general, the agreement between the VASP-MD and the Gaussian98 results is quite good, suggesting the validity of the approach followed for the G98 calculations.

Compared to adsorbed CO, the Au–C bond length in adsorbed COOH is longer, *i.e.* 1.983 Å *vs.* 2.095 Å, whereas the O–H bond length remains almost unchanged (see Table 3). Both C–O bond lengths in COOH have increased compared to CO, exhibiting values typical for carboxylic compounds (1.21 and 1.37 Å). The ν(Au–C) vibration frequency decreases from 338 cm^{-1} (CO/Au(110)) to 249 cm^{-1} (COOH/Au(110)).

Formation of COOH from CO and OH on Au(110). The energy profile of the reaction path for the formation of COOH from co-adsorbed CO and OH on Au(110) is shown in Fig. 3. The reaction coordinate plotted is the distance between the C in the CO fragment and the O in the OH fragment. The initial state represents CO adsorbed atop and OH adsorbed bridge within the same unit cell, as illustrated in the figure. In the final state, the carbon atom of the COOH is coordinated slightly off the atop site (see also Fig. 3). In the transition state, the OH is essentially above the long-bridge site next to the Au atom coordinating the CO. The reaction barrier with respect to the reactants within the same unit cell is 0.25 eV; with respect to the reactants at infinite separation (dashed line in Fig. 3), it is 0.57 eV. The energy gain (exothermicity) for the formation of COOH is 0.91 eV with respect to reactants within the same unit cell, and 0.69 eV with respect to the reactants at infinite separation.

The low barrier found for the CO + OH reaction is in agreement with recent calculations of CO + O reaction on gold by Liu *et al.*[11] They found that on Au(221), which is similar to (110), CO can readily react with co-adsorbed atomic O with a barrier of 0.25 eV.

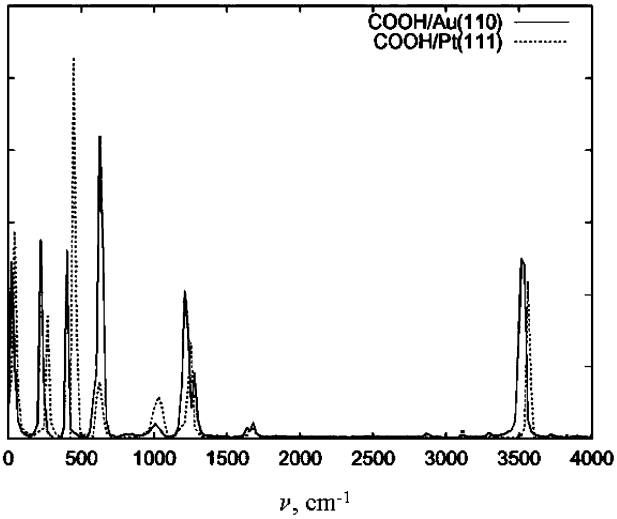

Fig. 2 Calculated vibrational power spectra for COOH adsorbed on Au(110) and Pt(111).

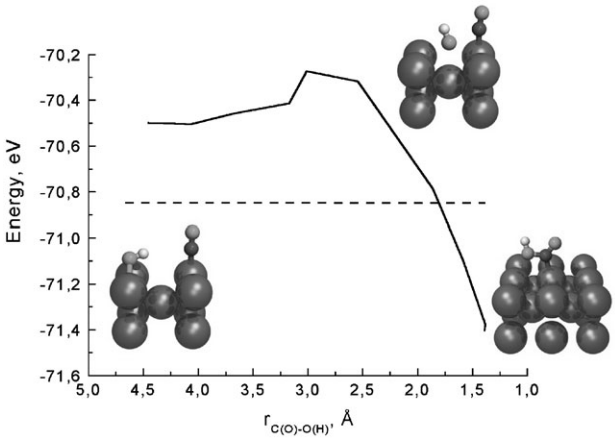

Fig. 3 Energy profile as function of the reaction coordinate for CO + OH on Au(110). The reaction coordinate is defined as a distance between C(O) and O(H). The dashed line shows the energy at infinite separation of CO and OH.

Table 4 COOH vibrational frequencies in cm^{-1}

	VASP	G98
Free	—	ν_{C-O} 1046; δ_{OH} 1275; $\nu_{C=O}$ 1819; ν_{OH} 3513
Adsorbed on Au(110)	ν_{COH} 1010; δ_{OH} 1230; ν_{CO} 1680; ν_{OH} 3530	ν_{Au-C} 249; ν_{COH} 957; δ_{OH} 1245; ν_{CO} 1748; ν_{OH} 3518
Adsorbed on Pt(111)	ν_{COH} 1040; δ_{OH} 1260; ν_{CO} 1670; ν_{OH} 3560	ν_{Pt-C} 308; ν_{COH} 1038; δ_{OH} 1244; ν_{CO} 1739; ν_{OH} 3559
Literature[63]	ν_{C-O} 1190–1075; δ_{OH} 1380–1280; $\nu_{C=O}$ 1800–1740; ν_{OH} 3580–3500	

Table 5 Binding properties of CO on Pt(111)

Adsorption site	Binding energy/eV	r(Pt–C)/Å	r(C–O)/Å	anh(VASP)		harm(G98)		MD
				ν_{PtC}/cm^{-1}	ν_{CO}/cm^{-1}	ν_{PtC}/cm^{-1}	ν_{CO}/cm^{-1}	ν_{CO}/cm^{-1}
Top	−1.631	1.849	1.156	452	2074	511	2104	2100
Bridge	−1.752	1.600	1.179	—	—	—	—	—
Hollow hcp	−1.798	1.481	1.189	—	—	—	—	—
Hollow fcc	−1.803	1.441	1.192	—	—	—	—	—

Pt(111)

Adsorption of CO and OH on Pt(111). Binding energies, geometries, and vibrational properties for CO and OH on the different adsorption sites of Pt(111) are collected in Tables 5 and 6. These systems have been extensively studied in the literature, and the results presented here agree with previous calculations. The DFT slab calculations predict the fcc site to be the most energetically favourable for CO on Pt(111), in disagreement with experiment. In fact, calculations predict the atop site to be the least favourable. This artifact of the DFT calculations has been discussed in detail in the literature.[55] Here, we focus on CO adsorbed on the atop site and compare the computed results with the available experimental data. As reported previously,[39] CO adsorbs on-top on Pt(111) with binding energy of *ca.* −1.6 eV relative to uncoordinated CO. The Pt–C and C–O bonds are 1.849 Å and 1.156 Å, respectively. The VASP computed vibrational frequencies are 452 cm^{-1} (for ν_{Pt-C}) and 2074 cm^{-1} (for ν_{C-O}), slightly lower than the frequencies obtained from cluster calculations, 511 cm^{-1} and 2104 cm^{-1}, respectively (Table 5). The VASP-computed frequencies agree well with the experimental values of 466 cm^{-1},[56] and 2084 cm^{-1}.[57]

In Table 6 the binding energies and properties of OH adsorbed on various sites on Pt(111) are collected. The calculations show that for OH adsorption there are two favourable sites, top and bridge with adsorption energies −2.33 and −2.26 eV, respectively. Since the difference in adsorption energy between these two sites is small (*ca.* 0.07 eV) we consider only the top site for CO + OH reaction study. The preference of OH for the atop coordination on Pt(111) is in good agreement with recent UHV experiments by Bedurftig *et al.*[58]

COOH adsorption on Pt(111). Tables 4 and 7 give the computed binding energy, geometry, and vibrational properties of COOH adsorbed on Pt(111). COOH adsorbs most favourably with the C atom coordinated to one Pt surface atom, with a binding energy of −2.39 eV, which is about 0.6 eV more negative (*i.e.* more favourable) than on Au(111). The adsorption geometry, as well as the vibrational properties, are very similar to COOH adsorbed on Au (Tables 4 and 7), as can be seen from the vibrational power spectrum shown as the dashed line in Fig. 2. The characteristic vibration modes for COOH adsorbed on the Pt(111) cluster are also presented in Table 4.

As in the case of Au(110), the Pt–C bond length in adsorbed COOH is elongated, *i.e.* 2.00 Å *vs.* 1.85 Å for the Pt–C bond in Pt–CO, whereas the O–H bond length, 0.98 Å, is similar to that in free COOH. Both C–O bond lengths in COOH have increased compared to CO, namely 1.21 Å (C–O) and 1.36 Å (C–OH). Also, the Pt–C vibration frequency decreases from 452–511 cm^{-1} for Pt(111)–CO to 308 cm^{-1} in Pt(111)–COOH.

Table 6 Binding properties of OH on Pt(111)

Adsorption site	Binding energy/eV	r(Pt–O)/Å	r(O–H)/Å	α
Atop	−2.330	2.001	0.981	145.0
Bridge	−2.262	1.728	0.985	111.6
hollow hcp	−1.792	1.638	0.980	180.0
hollow fcc	−1.897	1.592	0.980	178.9

Table 7 Binding properties of COOH on Pt(111)

Adsorption site	Binding energy/eV	r(Pt–C)/Å	r(C–O$_1$)/Å	r(C–O$_2$)/Å	r(O$_2$–H)/Å
C atop	−2.34	2.005	1.213	1.362	0.984

Formation of COOH from CO and OH on Pt(111). The energy profile of the reaction path for the formation of COOH from co-adsorbed CO and OH on Pt(111) is shown in Fig. 4. The reaction coordinate plotted is the distance between the C in the CO fragment and the O in the OH fragment. The initial state represents both CO and OH adsorbed atop within the same unit cell, as illustrated in the figure. In the final state, the carbon atom of the COOH is coordinated slightly off the atop site (see also Fig. 4). The reaction barrier with respect to the reactants within the same unit cell is 0.58 eV; with respect to the reactants at infinite separation (dashed line in Fig 4), it is 0.71 eV. The energy gain (exothermicity) for the formation of COOH is 0.60 eV with respect to reactants within the same unit cell, and 0.47 eV with respect to the reactants at infinite separation.

The result obtained for the barrier of the CO + OH reaction is in reasonable agreement with a similar DFT calculation carried out by Anderson and Neshev, who found 0.44 eV for the reaction on a 2-atom Pt cluster. It is also close to values computed for the CO + O reaction: Alavi *et al.*[59] found 0.65 eV for reactants in the same unit cell and 1.05 eV at infinite separation; Gong *et al.*[60] report 0.79 eV; whereas Eichler *et al.* report a value of 0.74 eV.[61,62]

Mechanistic implications and concluding remarks

The aim of this final section is to discuss to what extent the results presented above may aid in understanding the

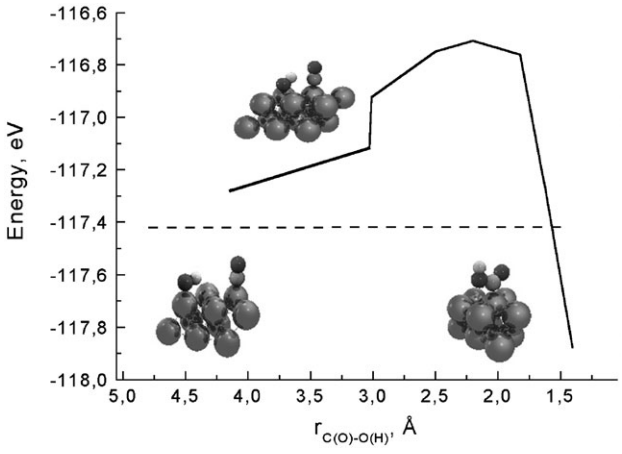

Fig. 4 Energy profile as a function of the reaction coordinate for CO + OH on Pt(111). The reaction coordinate is defined as a distance between C(O) and O(H). The dashed line shows the energy at infinite separation of CO and OH.

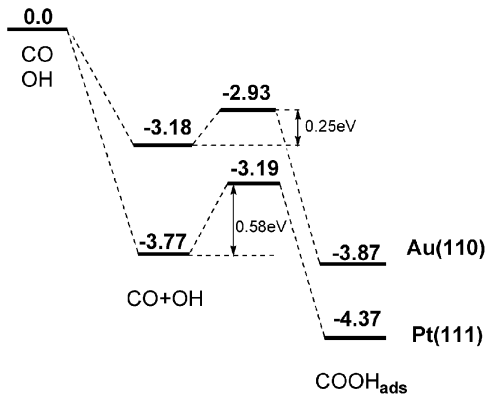

Fig. 5 Energy diagram for the CO and OH reaction on Au(110) and Pt(111) surfaces, energy is in eV relative to free CO and OH.

seemingly disparate CO oxidation kinetics on Pt and Au electrodes. To facilitate this discussion, the computed reaction profiles for the CO + OH reaction on Au(110) and Pt(111) are compared schematically in Fig. 5.

The figure illustrates the significantly lower activation energy for the CO + OH reaction on Au(110) compared to Pt(111). Even though we did not carry out similar calculations for the reaction on Pt(110) (the most active surface for the electrochemical CO oxidation[19]), we believe these mechanistic implications still generalize to the other surfaces of Au and Pt, including polycrystalline. On the (110) surface, one expects the binding of CO, OH, and COOH to be stronger, shifting the entire curve of Fig. 4 down in energy, presumably a bit more in favour of the CO + OH reactant side than the COOH product side. This implies that the activation energy would remain similar to, or even higher than on Pt(111), leaving the comparison with Au(110) intact. The DFT results for the CO + O reaction on Pt(111) and Pt(100) obtained by Eichler[62] indeed suggest that the more open Pt(100) surface has a slightly higher activation energy.

Even though the DFT results clearly point to a lower activation energy for the CO oxidation by OH on Au(110) compared to Pt, we do not believe that this fact in itself explains the surprisingly high activity of Au(110) for the electrochemical CO oxidation. However, Fig. 5 also indicates a qualitatively different kind of stabilization of the adsorbed COOH intermediate with respect to the adsorbed CO + OH fragments on the Au(110) surface, as compared to the Pt(111) surface. Although the formation energy of COOH from adsorbed CO and OH is similar on both surfaces (there is in fact a 0.1 eV extra stabilization on Au, but this number is insignificant as it is within the error bars of current DFT methods), the fact that the entire energy curve lies higher in energy for Au(110) suggests that the actual stability and corresponding surface coverage is high for COOH and low for CO on Au(110), but high for both on Pt(111). Therefore, COOH is expected to be stable on Au and Pt, but CO only on Pt. This stability of the COOH intermediate on gold may be an important reason for the activity of single-crystal gold in the electrochemical oxidation of CO at room temperature, as it would also explain why there is no need for small gold nanoparticles or an oxidic support under electrochemical conditions (in stark contrast to the gas-phase CO oxidation).

The energy difference calculated for the adsorbed CO + OH fragments between Au(110) and Pt(111) is mainly due to the different adsorption strengths for CO. Whereas CO is strongly adsorbed on Pt and leads to self-poisoning and the associated negative reaction order in CO solution concentration, on Au the CO adsorption is much weaker and the electrochemical CO oxidation rate exhibits the conventional positive reaction order in CO solution concentration. Therefore, Fig. 5 obviously explains the different reaction orders on both surfaces.

What remains to be discussed is whether the scheme in Fig. 5 could also aid in understanding the seemingly disparate role of OH in CO electro-oxidation on gold and platinum, as well as the experimental pH dependence. Whereas on Pt, CO oxidation takes place in the potential region at which OH is formed on the surface and exhibits a Tafel slope of *ca.* 75 mV dec^{-1}, on gold CO oxidation starts at potentials before any surface oxidation is evident and exhibits a Tafel slope close to 120 mV dec^{-1}. We believe the gold oxidation kinetics may be explained by two (at least apparently) alternative schemes. In the first scheme, one would still adhere to the necessity of forming OH on the surface, as suggested by Markovic *et al.*,[31] which should then be a rate-determining step as the potential for OH formation is unfavourable (note that OH adsorption is in fact slightly more favourable on Au(110) than on Pt(111); see Tables 2 and 6). This would, in principle, explain the Tafel slope of 120 mV dec^{-1}. Once formed, adsorbed OH rapidly reacts with adsorbed CO to COOH and CO_2, as suggested by the low barrier in Figs. 3 and 5. However, considering the low concentrations of both CO and OH on the surface in this scheme, it is difficult to imagine how this could lead the very substantial CO oxidation currents measured experimentally—CO oxidation would still be a slow reaction in this scheme. Also, we believe that there is no direct experimental evidence for the formation of surface-bonded OH on gold in the potential region of interest. An alternative scheme makes use of the above-mentioned relative stability of adsorbed COOH on Au. This stability in combination with the low barrier for the CO + OH reaction on gold may in fact suggest a reaction directly with water:

$$\underset{\text{(rate-determining step)}}{CO_{ads} + H_2O \rightarrow COOH_{ads} + H^+ + e^-} \quad (6)$$

$$COOH_{ads} \rightarrow CO_2 + H^+ + e^- \text{ (fast)} \quad (7)$$

Note the different rate-determining step in this mechanism compared to the mechanism discussed in the Introduction (reactions 4 and 5). This scheme would explain both the (apparent) absence of surface-bonded OH during CO oxidation as well as the 120 mV dec^{-1} Tafel slope. However, this scheme would not exhibit the experimentally observed pH dependence, as (at least formally) the rate of reaction 6 is not pH dependent. Unfortunately, a quantitatively accurate DFT calculation of the rate-determining step in this scheme, especially regarding any possible pH dependence, is still very expensive. It would require simulating a fully solvated proton at the metal–water interface and the inclusion of the electrode potential (however, for some initial simulations, see ref. 64).

The computed energy profile for the CO + OH reaction on Pt(111) is not in disagreement with the mechanism suggested for CO oxidation kinetics on Pt in the Introduction, *i.e.* reaction 1, 3 and 4. Surface-bonded CO on Pt is much more stable than on Au, and hence there is a substantial barrier associated with forming COOH from CO and OH. In the mechanisms suggested for both Au and Pt, surface-bonded COOH is formed *in or after* the rate-determining step, suggesting its concentration will be low and it should be very difficult to observe this species using *in situ* vibrational spectroscopy.

Acknowledgements

This work was financially supported by the Energy Research Center of the Netherlands (ECN) and the Netherlands Organization for Scientifc Research (NWO). We thank Peter Vassilev for performing the Fourier transformations.

References

1 C. Song, *Catal. Today*, 2002, **77**, 17–49.

2 T. Utaka, K. Sekizawa and K. Eguchi, *Appl. Catal.*, 2000, **194–195**, 21–26.
3 P.-Y. Lin, M. Skoglundh, L. Loewendahl, J.-E. Otterstedt, L. Dahl, K. Jansson and M. Nygren, *Appl. Catal.*, 1995, **6**, 237–254.
4 M. Skoglundh, P. Thormahlen, E. Fridell, F. Hajbolouri and E. Jobson, *Chem. Eng. Sci.*, 1999, **54**, 4559–4566.
5 J. T. Kummer, *J. Phys. Chem.*, 1986, **90**, 4747–4752.
6 I. Langmuir, *Trans. Faraday Soc.*, 1921, **17**, 621.
7 (*a*) M. Valden, X. Lai and D. W. Goodman, *Science (Washington, D. C.)*, 1998, **281**, 1647–1650; (*b*) A. K. Santra and D. W. Goodman, *Electrochim. Acta*, 2002, **47**, 3595–3609.
8 W. A. Bone and R. A. Wheeler, *Philos. Trans*, 1906, **206A**, 1.
9 W. A. Bone and G. W. Andrew, *Proc. R. Soc. London, Ser. A*, 1925, **109**, 409.
10 (*a*) M. Haruta, *Catal. Today*, 1997, **36**, 153–166; (*b*) A. Sanchez, S. Abbet, U. Heiz, W.-D. Schneider, H. Häkkinen, R. N. Bartlett and U. Landman, *J. Phys. Chem. A*, 1999, **103**, 9573–9578.
11 (*a*) Z.-P. Liu, P. Hu and A. Alavi, *J. Am. Chem. Soc*, 2002, **124**, 14770–14779; (*b*) N. López and J. K. Nørskov, *J. Am. Chem. Soc.*, 2002, **124**, 11262–11263; (*c*) L. M. Molina and B. Hammer, *Phys. Rev. Lett.*, 2003, **90**, 206102.
12 G. Hoogers and D. Thompsett, *Cattech*, 2000, **3**, 106–124.
13 L. Carrette, K. A. Friedrich and U. Stimming, *Fuel Cells*, 2001, **1**, 5–39.
14 S. Gilman, *J. Phys. Chem.*, 1964, **68**, 70–80.
15 G. Q. Lu, P. Waszczuk and A. Wieckowski, *J. Electroanal. Chem.*, 2002, **532**, 49–55.
16 N. M. Markovic, B. N. Grgur, C. A. Lucas and P. N. Ross, *J. Phys. Chem. B*, 1999, **103**, 487–495.
17 M. T. M. Koper, A. P. J. Jansen, R. A. van Santen, J. J. Lukkien and P. A. J. Hilbers, *J. Chem. Phys.*, 1998, **109**, 6051–6062.
18 T. J. Schmidt, P. N. Ross and N. M. Markovic, *J. Phys. Chem. B*, 2001, **105**, 12082–12086.
19 N. P. Lebedeva, M. T. M. Koper, J. M. Feliu and R. A. van Santen, *J. Phys. Chem.*, 2002, **106**, 12938–12947.
20 M. T. M. Koper, T. J. Schmidt, N. M. Markovic and P. N. Ross, *J. Phys. Chem. B*, 2001, **105**, 8381–8386.
21 W. B. Wang, M. S. Zei and G. Ertl, *Phys. Chem. Chem. Phys.*, 2001, **3**, 3307–3311.
22 J. Lee, W. B. Wang, M. S. Zei and G. Ertl, *Phys. Chem. Chem. Phys.*, 2002, **4**, 1393–1397.
23 T. H. M. Housmans, J. M. Feliu and M. T. M. Koper, *J. Electroanal. Chem*, 200410.1016/j.elechem.2004.06.003, in press.
24 A. M. El-Aziz and L. A. Kibler, *J. Electroanal. Chem.*, 2002, **534**, 107–114.
25 N. P. Lebedeva, M. T. M. Koper, J. M. Feliu and R. A. van Santen, *J. Electroanal. Chem.*, 2002, **524–525**, 242–251.
26 E. Santos, E. P. M. Leiva and W. Vielstich, *Electrochim. Acta*, 1991, 555–561.
27 E. Herrero, J. M. Feliu, S. Blais, Z. Radovic-Hrapovic and C. Jerkiewicz, *Langmuir*, 2000, 4779–4783.
28 Y. Zhu, H. Uchida and M. Watanabe, *Langmuir*, 1999, **15**, 8757–8764.
29 M. Watanabe, Y. Zhu and H. Uchida, *J. Phys. Chem. B*, 2000, **104**, 1762–1768.
30 G. J. Edens, A. Hamelin and M. J. Weaver, *J. Phys. Chem. B*, 1996, **100**, 2322–2329.
31 B. Blizanac, C. A. Lucas, M. E. Gallagher, M. A. Arenz, P. N. Ross and N. M. Markovic, *J. Phys. Chem. B*, 2004, **108**, 625–634.
32 A. B. Anderson and N. M. Neshev, *J. Electrochem. Soc.*, 2002, **149**, E383–E386.
33 C. Saravanan, B. D. Dunietz, N. M. Markovic, G. Somorjai, P. N. Ross and M. Head-Gordon, *J. Electroanal. Chem*, 2003, **554–555**, 459–465.
34 Y. Ishikawa, M.-S. Liao and C. R. Cabrera, *Surf. Sci.*, 2002, **513**, 98–110.
35 Y. Ishikawa, M. S. Liao and C. R. Cabrera, *Surf. Sci.*, 2000, **463**, 66–80.
36 G. Kresse and J. Hafner, *Phys. Rev. B*, 1993, **47**, 558–561.
37 G. Kresse and J. Hafner, *Phys. Rev. B*, 1994, **49**, 14251–14269.
38 G. Kresse and J. Hafner, *Comput. Mater. Sci.*, 1996, **6**, 15.
39 M. T. M. Koper, T. E. Shubina and R. A. van Santen, *J. Phys. Chem. B*, 2002, **106**, 686–692.
40 S. H. Vosko, L. Wilk and M. Nusair, *Can. J. Phys.*, 1980, **58**, 1200–1211.
41 J. P. Perdew, J. A. Chevary, S. H. Vosko, K. A. Jackson, M. R. Pederson, D. J. Singh and C. Fiolhais, *Phys. Rev. B*, 1992, **46**, 6671–6687.
42 M. C. Payne, M. P. Teter, D. C. Allen, T. C. Allen and J. D. Joannopoulos, *Rev. Mod. Phys.*, 1992, **64**, 1045–1097.
43 D. Vanderbilt, *Phys. Rev. B*, 1990, **41**, 7892–7895.
44 *Structure data of Elements and Intermetallic phases*, Springer, Berlin, 1977, Vol IIIb.
45 E. L. Meijer, R. A. van Santen and A. P. J. Jansen, *J. Phys. Chem.*, 1996, **100**, 9282–9291.
46 E. L. Meijer, PhD Thesis, Eindhoven University of Technology, 2000.
47 M. Allen and D. Tildesley, *Computer Simulation of Liquids*, Clarendon Press, Oxford, 1987.
48 M. J. Frisch, G. W. Trucks, H. B. Schlegel, G. E. Scuseria, M. A. Robb, J. R. Cheeseman, V. G. Zakrzewski, J. J. A. Montgomery, R. E. Stratmann, J. C. Burant, S. Dapprich, J. M. Millam, A. D. Daniels, K. N. Kudin, M. C. Strain, O. Farkas, J. Tomasi, V. Barone, M. Cossi, R. Cammi, B. Mennucci, C. Pomelli, C. Adamo, S. Clifford, J. Ochterski, G. A. Petersson, P. Y. Ayala, Q. Cui, K. Morokuma, D. K. Malick, A. D. Rabuck, K. Raghavachari, J. B. Foresman, J. Cioslowski, J. V. Ortiz, B. B. Stefanov, G. Liu, A. Liashenko, P. Piskorz, I. Komaromi, R. Gomperts, R. L. Martin, D. J. Fox, T. Keith, M. A. Al-Laham, C. Y. Peng, A. Nanayakkara, C. Gonzalez, M. Challacombe, P. M. W. Gill, B. Johnson, W. Chen, M. W. Wong, J. L. Andres, C. Gonzalez, M. Head-Gordon, E. S. Replogle and J. A. Pople, *Gaussian Inc.*, Pittsburgh PA, 1999.
49 A. D. Becke, *Phys. Rev. A*, 1988, **38**, 3098–3100.
50 C. Lee, W. Yang and R. G. Parr, *Phys. Rev. B*, 1988, **37**, 785–789.
51 A. D. Becke, *J. Chem. Phys.*, 1993, **98**, 5648.
52 B. Beden, A. Bewick, K. Kunimatsu and C. Lamy, *J. Electroanal. Chem.*, 1982, **142**, 345–356.
53 M. A. Tadayyoni and M. J. Weaver, *Langmuir*, 1986, **2**, 179–183.
54 Y. Zhang and M. J. Weaver, *J. Electroanal. Chem.*, 1993, **354**, 173–183.
55 (*a*) P. J. Feibelman, B. Hammer, J. K. Norskov, F. Wagner, M. Scheffler, R. Stumpf, R. Watwe and J. Dumesic, *J. Phys. Chem. B*, 2001, **105**, 4018–4025; (*b*) A. Gil, A. Clotet, J. M. Ricart, G. Kresse, M. García-Hernández, N. Rösch and P. Sautet, *Surf. Sci.*, 2003, **530**, 71; (*c*) G. Kresse, A. Gil and P. Sautet, *Phys. Rev. B*, 2003, **68**, 73401.
56 D. Hoge, M. Tüshaus, E. Schweizer and A. M. Bradshaw, *Chem. Phys. Lett.*, 1988, **151**, 230–235.
57 M. S. Tüshaus, E. Schweizer, P. Hollins and A. M. Bradshaw, *J. Electron. Spectrosc. Relat. Phenom.*, 1987, **44**, 305–316.
58 K. Bedurfig, S. Volkening, Y. Wang, J. Wintterlin, K. Jacobi and G. Ertl, *J. Chem. Phys.*, 1999, **111**, 11147–11154.
59 X.-G. Gong, Z.-P. Liu, R. Raval and P. Hu, *J. Am. Chem. Soc.*, 2004, **126**, 8–9.
60 A. Alavi, P. Hu, T. Deutsch, P. L. Silvestrelli and J. Hutter, *Phys. Rev. Lett.*, 1998, **80**, 3650–3653.
61 A. Eichler and J. Hafner, *Phys. Rev. B*, 1999, **59**, 5960–5967.
62 A. Eichler, *Surf. Sci.*, 2002, **498**, 314–320.
63 N. B. Colthup, L. H. Daly and S. E. Wiberley, *Introduction to infrared and Raman spectroscopy*, Academic Press: New York and London, 1964.
64 S. Desai and M. Neurock, *Electrochim. Acta*, 2003, **48**, 3759–3773.